The spatial footprint of injection wells in a global compilation of induced earthquake sequences

T.H.W. Goebel, E.E. Brodsky - *University of California, Santa Cruz*

This research is supported by U.S. Department of Energy grant DE-SC0015539

Objectives

Fluid injection can cause extensive earthquake activity, at times at unexpectedly large distances. Appropriately mitigating associated seismic hazards requires a better understanding of the zone of influence of injection. We analyze spatial seismicity decay in a global dataset of 18 induced cases with clear association between isolated wells and earthquakes. Our global compilation of fluid-injection induced seismicity allows for a better understanding of the maximum earthquake-triggering-distance from an injection site.

Key findings

1. We identify two induced event populations: (i) sequences with near-well seismicity density plateau and abrupt decay, dominated by square-root space-time migration and pressure diffusion. (ii) Sequences with exhibits larger spatial footprints and power law-like spatial decay over more than 10 km.
2. Injection at sites with abrupt decay occurs within the crystalline basement and show smaller maximum magnitude events.
3. The maximum magnitude is larger for sites with steady decay due to the greater probability of activating bigger faults within the extended spatial footprint of the injection wells.
4. Far-reaching poroelastic effects increase seismic hazard beyond expectations from purely pressure-driven seismicity.

1. Observations of induced events at large distance from injectors

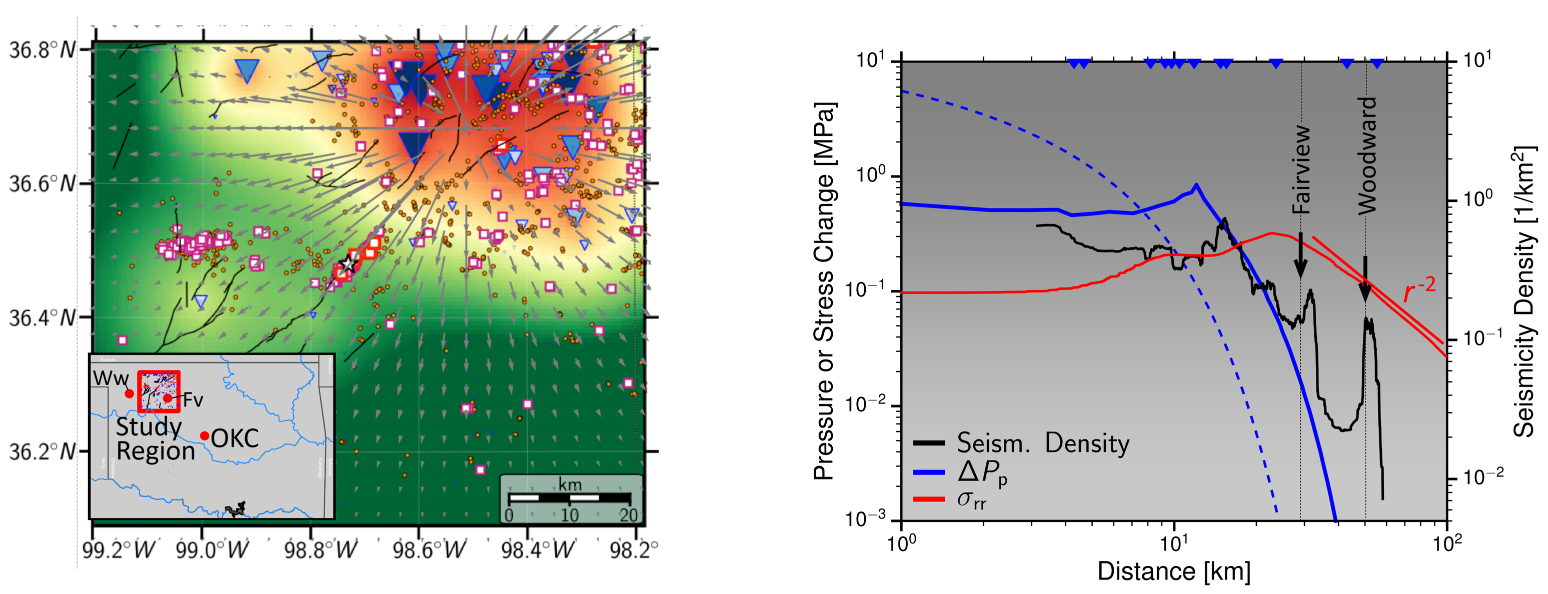

Example of far-field induced earthquakes and expected shape of pore-pressure (blue curves), and poroelastic stresses (red curve) and observed seismicity decay in Fairview, Oklahoma.

2. Induced seismicity data compilation

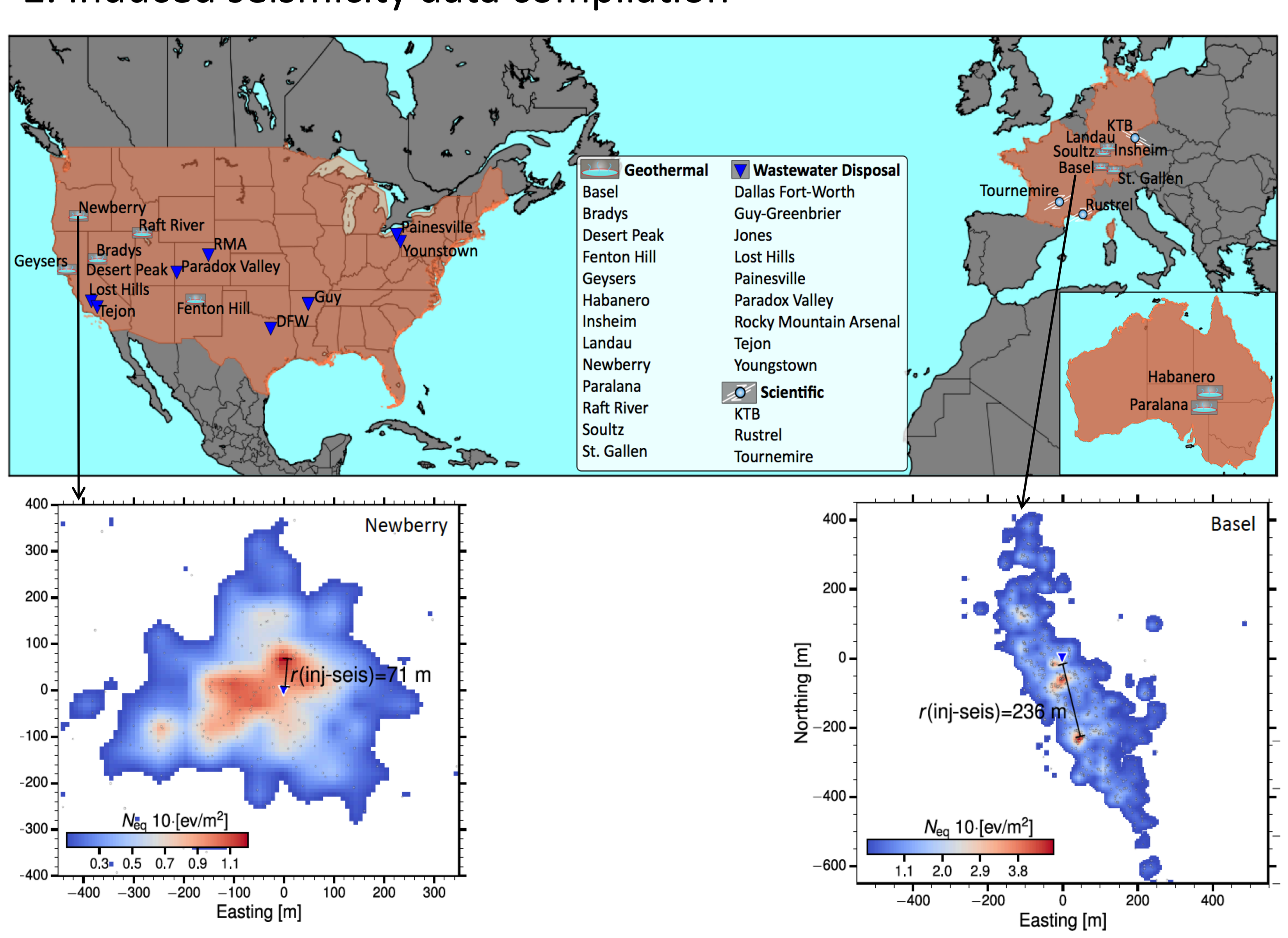

We based our initial site selection on a compilation by Wilson et al. from which we identified point-source injectors that were not related to hydraulic fracturing which was excluded because of the more complex inelastic fluid-rock coupling close to the borehole. We confirmed with previous publications that seismic events were connected to a single injection well and then performed a detailed data quality assessment of the seismicity data. Fluid injection operations include wastewater (blue triangles), geothermal (light-blue ellipse) and scientific (white arrows) wells.

3. Seismicity density decay from injection wells

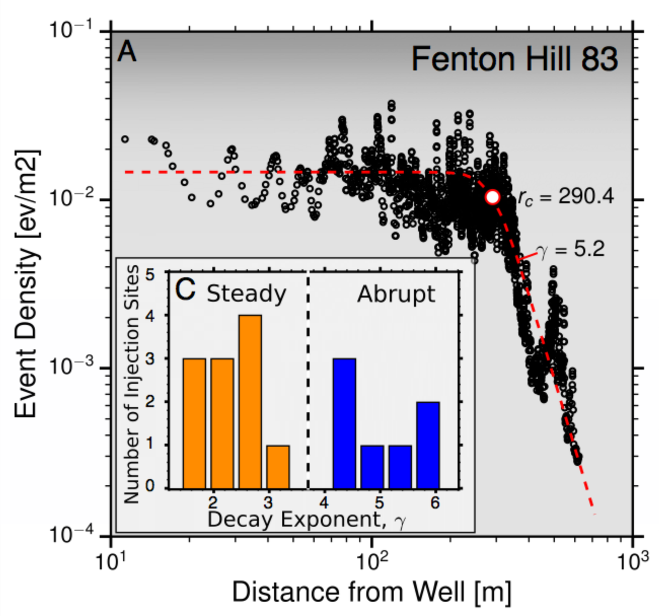

Examples of functional fits to the observed spatial densities at the Fenton Hill (A) and Paradox Valley (B) injection sites. Based on the distance decay exponent γ, we differentiate sites with steady decay with γ between 1.5 and 3.1 and abrupt decay with γ between 4.3 and 5.9 (see inset).

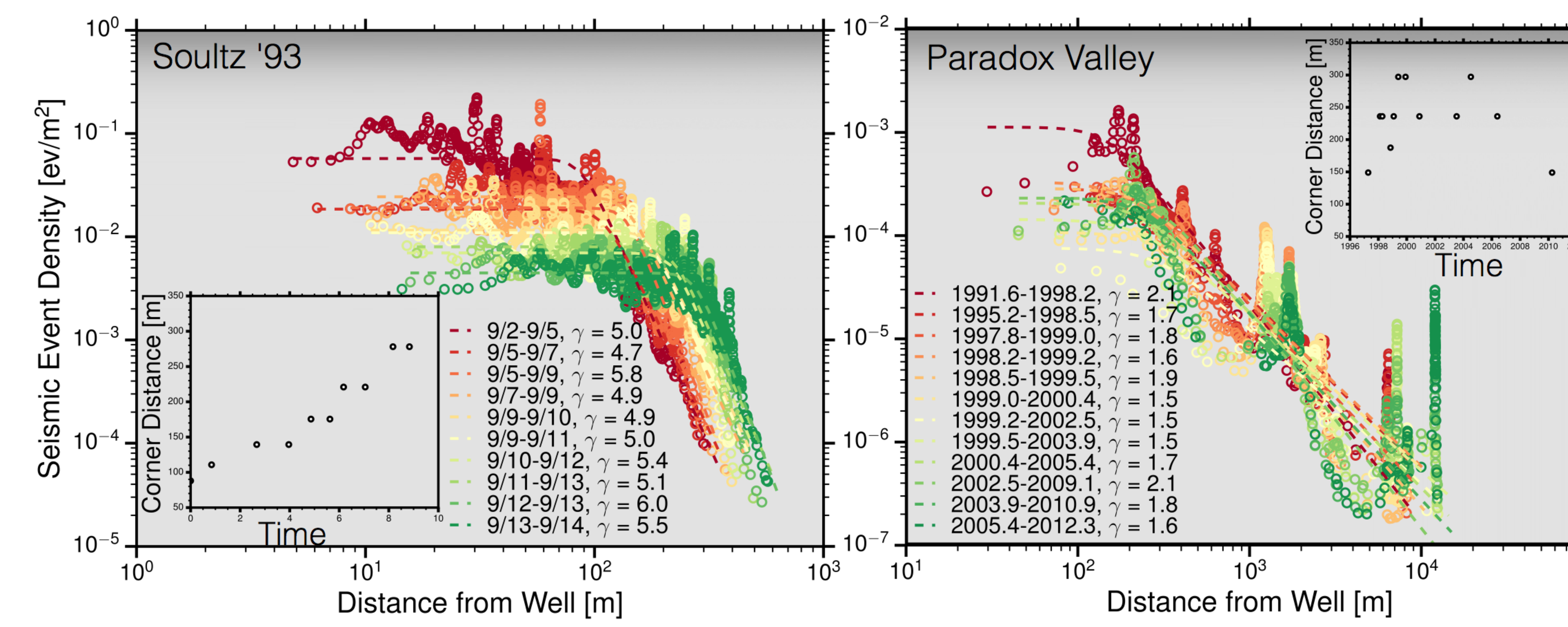

The shape of spatial decay is time invariant as exemplified for the Soultz (left) and Paradox Valley injection sites (right). The shape and exponent of spatial decay remains relatively stable throughout the analyzed time periods (see legend for value of γ). The insets show changes in corner distance with time. Corner distances increase systematically with progressing injection in Soultz and show no systematic variation at the Paradox Valley site.

4. Separation into sequences with steady and abrupt decay

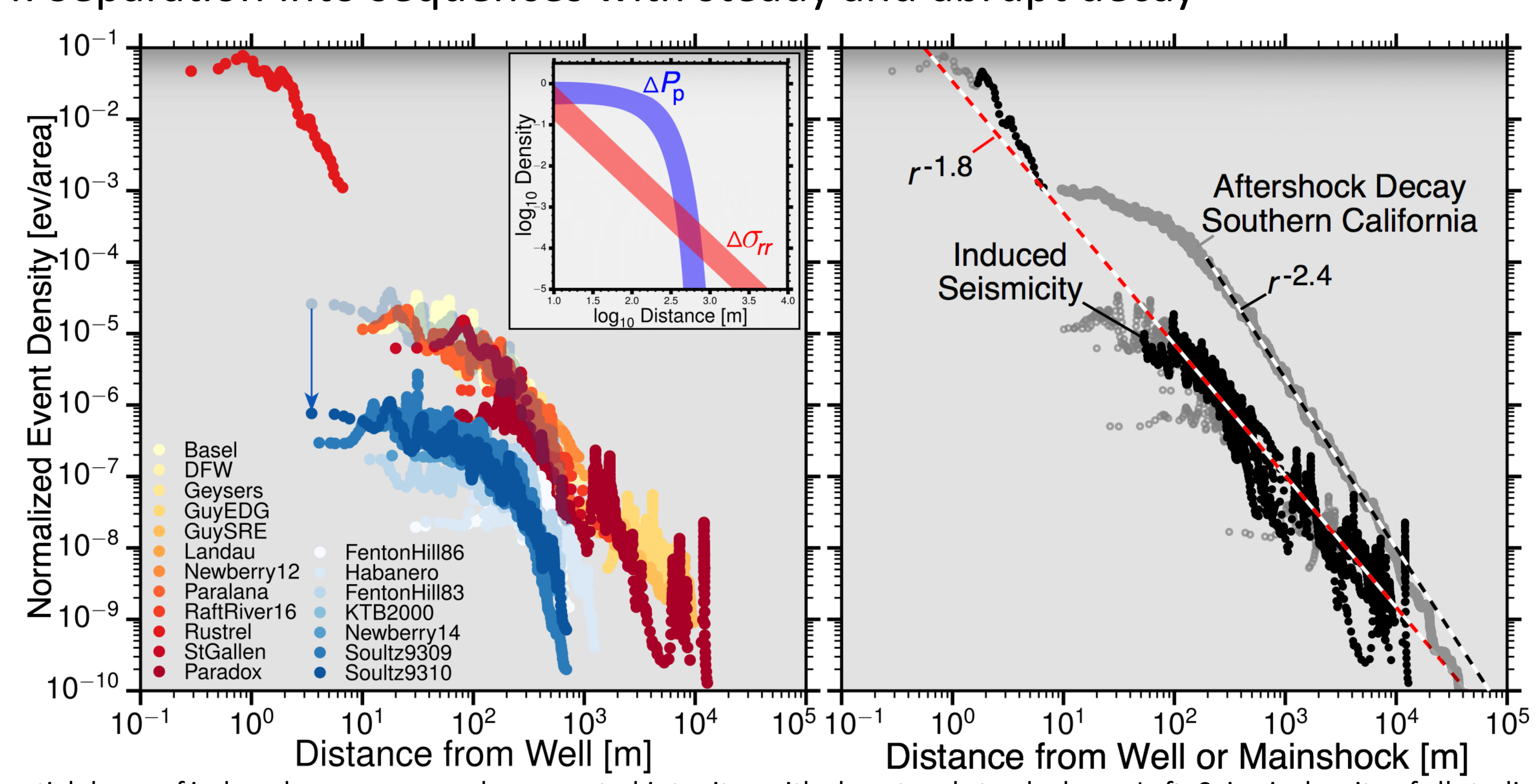

The spatial decay of induced sequences can be separated into sites with abrupt and steady decay. Left: Seismic density of all studied induced sequences, normalized by number of events above completeness. We show cases with abrupt decay in blue and steady decay in red colors. Inset: Theoretical expectation of spatial density fall-off, for which the blue curve shows the abrupt decay of pressure dominated sites and the red curve shows a power law decay for sites with strong poroelastic coupling. Right: Merged densities above r_c for sequences with steady decay (black markers) and power law fit (red, dashed line) with $\sim r^{-1.8}$ which is more gradual than the spatial decay of aftershocks.

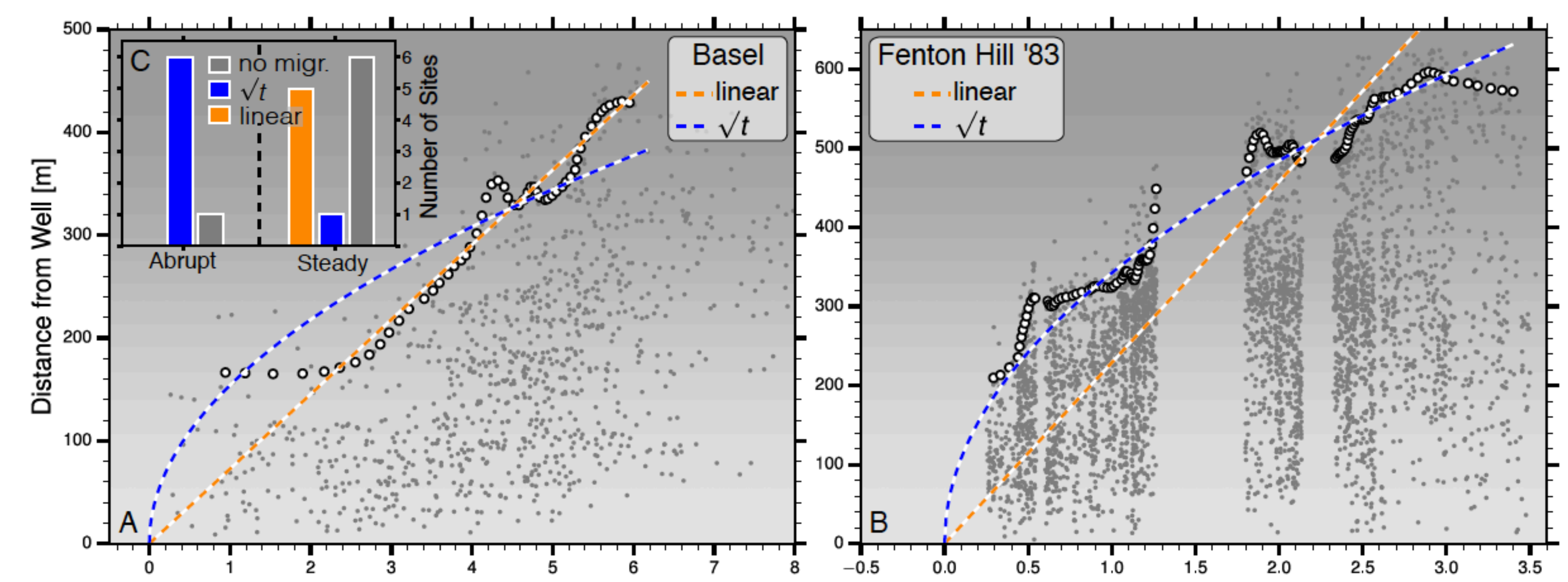

Sequences with abrupt spatial decay are dominated by square-root migration, an indication for pressure diffusion. Examples of linear (A) and square-root migration (B). Gray markers are event time and distance from injection, white markers show the 95th percentile of distances in specific time bins. (C) Number of sites with abrupt and steady decay with square-root (blue), linear (orange) or no migration (gray).

5. Injection depth and maximum magnitude

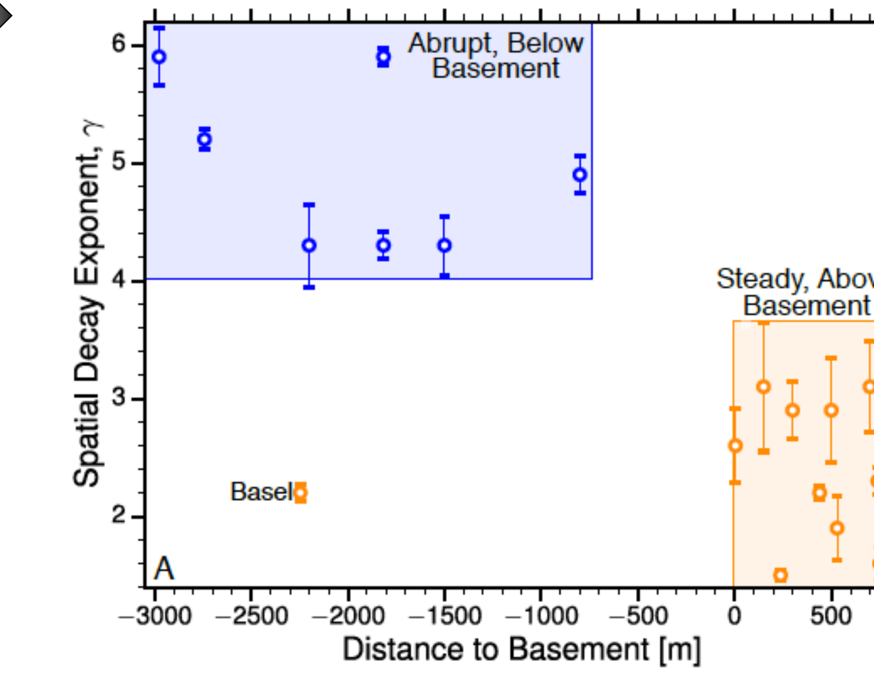

The spatial decay separated into abrupt (blue) and steady (orange) decay is controlled by the distance between injection and crystalline basement.

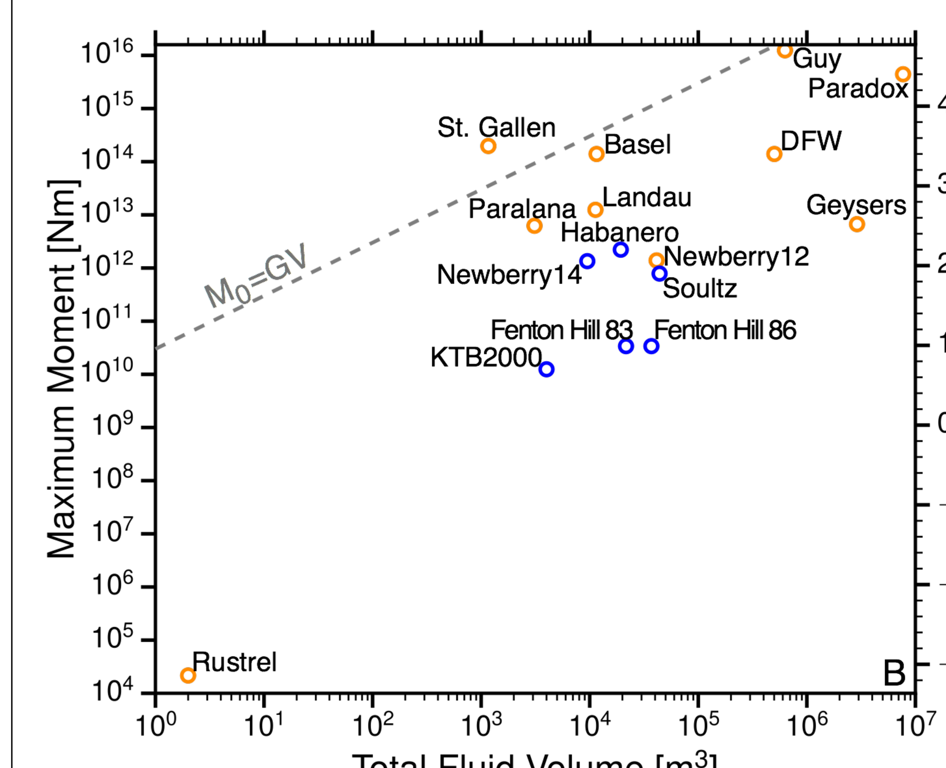

Maximum magnitude of each sequence as a function of total injected volume for steady (orange) and abrupt decays (blue). The dashed line is the theoretically expected maximum moment based on McGarr, 2014, for which G is shear modulus and V is total injected volume.

6. Spatial injection footprint and seismic hazard

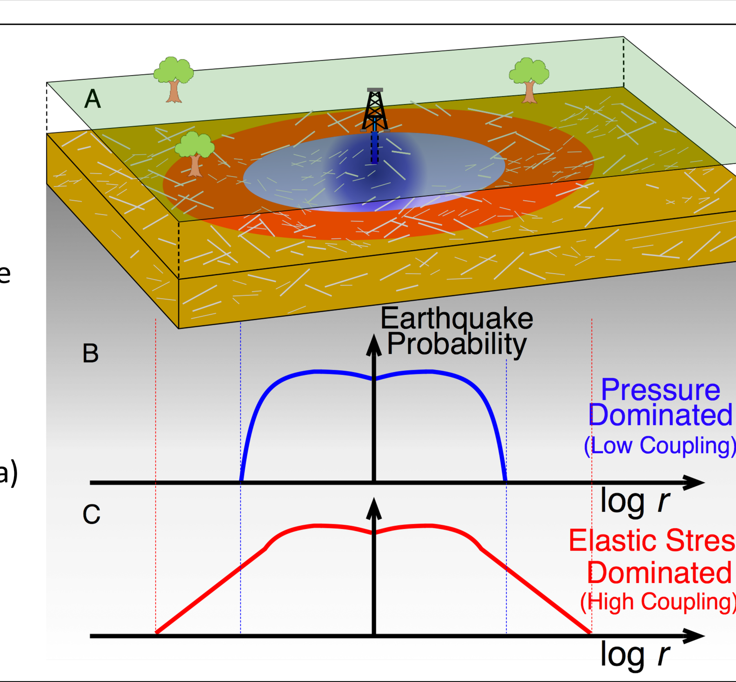

The probability of inducing an earthquake at distance r is controlled by fault availability and amplitude of stress perturbation. A) Schematic representation of injection operation and footprint of poroelastic response (blue and red ellipses) and fault network (gray lines). B) Earthquake probability (in events/area) as a function of distance from the injection well for pressure dominated triggering. C) Same as (B) in a coupled system with elastic stress dominance in the far-field. (axes in B and C are logarithmic)

7. Conclusion

Previous induced seismicity mitigation strategies encouraged injecting in sedimentary units instead of directly into the basement. However, our results suggest that injection into sedimentary rocks leads to more distant and larger earthquakes for a given volume of injection, perhaps due to more efficient pressure and stress transmission. The larger spatial footprints of above-basement injection may be responsible for the extensive seismogenic response in some areas such as Alberta and Oklahoma.

References

Goebel, T.H.W. & E.E. Brodsky. The spatial footprint of injection wells in a global compilation of induced earthquake sequences, Science (in press)

Goebel, T.H.W., Weingarten, M., Chen, X., Haffener, J., and Brodsky, E.E., 2017, The 2016 Mw5.1 Fairview, Oklahoma earthquakes: Evidence for long-range poroelastic triggering at >40 km from fluid disposal wells: Earth and Planetary Science Letters, v. 472, p. 50–61, doi: 10.1016/j.epsl.2017.05.011.

McGarr, A., 2014, Maximum magnitude earthquakes induced by fluid injection: Journal of Geophysical Research: Solid Earth, v. 119, p. 1–12, doi: 10.1002/2013JB010597.Received.

Wilson, M.P., Foulger, G.R., Gluyas, J.G., Davies, R.J., and Julian, B.R., 2017, HiQuake : The Human-Induced Earthquake Database: Seismological Research Letters, v. 88, no. 6, p. 1560–1565, doi: 10.1785/0220170112.